

Imaging the Molecular Disk Orbiting the Twin Young Suns of V4046 Sgr

David R. Rodriguez¹, Joel H. Kastner², David Wilner³, & Chunhua Qi³

ABSTRACT

We have imaged the disk surrounding the nearby ($D \sim 73$ pc), ~ 12 Myr, classical T Tauri binary system V4046 Sgr with the Submillimeter Array (SMA) at an angular resolution of $\sim 2''$. We detect a rotating disk in $^{12}\text{CO}(2-1)$ and $^{13}\text{CO}(2-1)$ emission, and resolve the continuum emission at 1.3 mm. We infer disk gas and dust masses of ~ 110 and ~ 40 Earth masses, respectively. Fits to a power-law disk model indicate that the molecular disk extends to ~ 370 AU and is viewed at an inclination of between $\sim 33^\circ$ and $\sim 39^\circ$ for dynamical stellar masses ranging from $1.8 M_\odot$ down to $1.5 M_\odot$ (the range of total mass previously determined for the central, 2.4 day spectroscopic binary). This range of disk inclination is consistent with that assumed in deducing the central binary mass (i.e., 35°), suggesting that the V4046 Sgr binary system and its circumbinary, molecular disk are coplanar. In light of the system's age and binarity, the presence of an extensive molecular disk orbiting V4046 Sgr provides constraints on the timescales of processes related to Jovian planet formation, and demonstrates that circumbinary Jovian planets potentially could form around close binary systems.

Subject headings: circumstellar matter — stars: binaries, individual (V4046 Sgr) — stars: pre-main sequence — stars: planetary systems — radio lines : stars

1. Introduction

Circumstellar disks around young stars serve both as the sources of material for accreting young stars and as the sites of nascent planets orbiting such stars. Numerous studies of such

¹Dept. of Physics & Astronomy, University of California, Los Angeles 90095, USA
(drodrigu@astro.ucla.edu)

²Center for Imaging Science, Rochester Institute of Technology, 54 Lomb Memorial Drive, Rochester NY 14623 (jkh@cis.rit.edu)

³Harvard-Smithsonian Center for Astrophysics, 60 Garden Street, Mail Stop 42, Cambridge, MA 02138
(dwilner@cfa.harvard.edu & cqi@cfa.harvard.edu)

disks have exploited photometry and spectroscopy of dust emission, as manifest in the form of a thermal infrared excess above the stellar continuum, to ascertain fundamental properties such as disk dimensions, density structure, dust mass, and dust grain composition (e.g., Zuckerman 2001; Dullemond et al. 2007, and references therein). Observations that can establish the composition and evolution of the *gaseous* component within circumstellar disks around pre-MS and young MS stars, meanwhile, are essential if we are to understand the processes involved in Jovian planet formation and the origins of comets and Kuiper Belt objects (Luu & Jewitt 2002; Hubbard, Burrows, & Lunine 2002; Ehrenfreund & Charnley 2000). For example, the near-IR lines of rovibrational H₂ and CO generally probe the terrestrial planet formation zones ($\lesssim 2$ AU) of gas disks, interior to the regions where Jovian planets are expected to form (e.g., Salyk et al. 2007; Najita et al. 2008; Bary et al. 2008; however, see Brittain et al. 2009). Mid-IR pure rotational lines of H₂ (Bitner et al. 2007, 2008; Najita et al. 2010) and rovibrational lines of H₂O, C₂N₂, and OH (Glassgold et al. 2009, and references therein) are potentially diagnostic of molecular gas mass and excitation in the innermost Jovian planet-forming zones, and also provide limited information concerning the structure, dynamics, and chemistry of these regions.

Sensitive measurements of (sub)millimeter-wave radio emission from orbiting CO (after H₂, the most abundant molecular species) around “isolated,” young (age ~ 5 –20 Myr), nearby ($D \lesssim 100$ pc) stars — with TW Hya as archetype — are key in this regard (Zuckerman et al. 1995; Kastner et al. 1997; Thi et al. 2004). Such stars are old enough that Jovian planets may already be forming or have formed in their circumstellar disks (e.g., Papaloizou & Nelson 2005; Thommes et al. 2008), and they are close enough for intensive follow-up study via interferometric molecular line imaging surveys. Though CO detections of the disks around pre-main sequence stars of such advanced ages are exceedingly rare thus far, (sub)millimeter-wave molecular imaging studies of the handful of known ~ 10 Myr-old molecular disks that lie within ~ 100 pc of Earth have yielded a wealth of information concerning the structure and evolution of gaseous, planet-forming disks (e.g., Qi et al. 2004, 2006, 2008; Hughes et al. 2008).

V4046 Sgr is one such isolated, “old,” nearby star system (age ~ 12 Myr, distance ~ 73 pc; Torres et al. 2008). The V4046 Sgr system is especially noteworthy in that it consists of a close ($\sim 9 R_{\odot}$ separation, 2.4-day period) pair of $\sim 0.9 M_{\odot}$ stars that are evidently still actively accreting mass (Stempels & Gahm 2004, and references therein). A previous molecular emission line survey with the Institut de Radio Astronomie Millimetrique (IRAM) 30-m telescope established the presence of CO, HCN, CN, and HCO⁺ within the dusty disk encircling the system (Kastner et al. 2008b). This makes V4046 Sgr only the fourth known example (after TW Hya, 49 Cet, and HD 141569; Zuckerman et al. 1995) of a pre-main sequence star within ~ 100 pc that possesses a molecular disk; V4046 Sgr is the only known

close-separation binary among them (HD 141569 has a pair of M-type companions, ~ 800 AU from the disk-bearing primary, see Weinberger et al. 2000). To confirm that the CO emission detected toward V4046 Sgr with the IRAM 30-m indeed arises in an orbiting, circumbinary disk, and to establish or constrain fundamental system parameters such as disk dimensions and inclination, we observed V4046 Sgr with the Submillimeter Array (SMA; Ho et al. 2004).

2. Observations

We obtained data in the SMA’s extended (28–226 m baselines) and compact (6–70 m baselines) configurations on 23 Feb. and 25 April 2009, respectively. The weather conditions were excellent on both nights. During each track, the receivers were tuned to provide simultaneous coverage of the $^{12}\text{CO}(2-1)$, $^{13}\text{CO}(2-1)$, and $\text{C}^{18}\text{O}(2-1)$ transitions as well as adjacent (1.3 mm) continuum, with the spectral backends configured to provide velocity resolution of 0.26 km s^{-1} . The data were edited and calibrated using the MIR software package¹. The passband response was calibrated using the quasars 3C 273 and 1924-292 for the extended configuration and 3C 84, 1924-292, and Uranus for the compact configuration. The antenna gain calibration was performed using 1924-292 (extended) and 1733-130 (compact). The flux scale was determined by bootstrapping observations of 3C 273 and Uranus and is accurate at the $\sim 10\%$ level. The continuum was determined using the line-free channels in both upper and lower sidebands for both configurations. From these data we determine a 1.3 mm continuum flux of $360 \pm 36 \text{ mJy}$.

We combined the extended and compact configuration data to produce a synthesized beam size of $2.2'' \times 1.5''$ at the 230 GHz frequency of $^{12}\text{CO}(2-1)$. Similarly, for $^{13}\text{CO}(2-1)$ we produced a synthesized beam size of $2.3'' \times 1.7''$ at its 220 GHz frequency. No C^{18}O 219 GHz emission was detected with a 3σ upper limit of 0.3 Jy beam^{-1} (synthesized beam size was $2.4'' \times 1.7''$). The standard tasks (CLEAN algorithm) of deconvolution and image restoration were performed with the MIRIAD software package. Images of the continuum and ^{12}CO were created using Briggs weighting (robust=0 and 1, respectively) for the visibilities. To reduce image noise, the ^{13}CO and C^{18}O images were generated using natural weighting. The complete observing parameters are listed in Table 1.

¹See <http://cfa-www.harvard.edu/~cqi/mircook.html>

3. Results

3.1. CO line maps

The resulting sequences of velocity-resolved SMA $^{12}\text{CO}(2-1)$ and $^{13}\text{CO}(2-1)$ images are displayed in Fig. 1. The contours start at 3 and 2 times the rms noise level, respectively, and increase as described in the figure caption. These images vividly demonstrate that the CO emission from V4046 Sgr arises from a rotating disk. The radial extent of the molecular disk is $\sim 5''$, or ~ 370 AU at the estimated 73 pc distance to V4046 Sgr. The similar overall extent of the CO emission in the N-S and E-W directions, coupled with the profound change in emission morphology with radial velocity, indicates that the disk is viewed at intermediate inclination (compare with, e.g., Fig. 3 in Beckwith & Sargent 1993, which illustrates a Keplerian molecular disk model viewed at an inclination of $\sim 45^\circ$). The channel map closest to the systemic LSR velocity ($V_{sys} \sim 2.9$ km s $^{-1}$) indicates a disk position angle (PA) on the sky of $\sim 75^\circ$, measured east of north. This PA is similar to that inferred for the dust disk from the 230 GHz continuum emission detected and resolved by the SMA (see § 3.3). We further refine these estimates for disk inclination, PA, and V_{sys} in § 4.1.

3.2. CO line profiles

The SMA $^{12}\text{CO}(2-1)$ and $^{13}\text{CO}(2-1)$ emission line profiles, as obtained by spatially integrating the line intensity maps within a $6''$ radius circular aperture, are highly symmetric (Figures 2 and 3). This confirms that the asymmetric appearance of the CO line profiles obtained with the IRAM 30-m telescope (Kastner et al. 2008b) was a consequence of slight mispointing (the 30-m data were obtained at very low source elevation, $\sim 15-20^\circ$, due to the southerly declination of V4046 Sgr) combined with the spatial resolution of the source by the 30-m beam, as opposed to significant density or temperature inhomogeneities intrinsic to the molecular disk.

3.3. 1.3 mm dust continuum emission

The continuum emission from the dust is partially resolved (Figure 4). Using MIRIAD, we fit an elliptical gaussian to the continuum visibilities to estimate the size and shape of the emission. The best fit yields major and minor axes of $1.10''$ and $0.93''$, respectively, with a position angle of $73 \pm 5^\circ$ east of north. This position angle is consistent with that inferred from the CO maps (§4.1). There is negligible contribution from the ($< 0.1''$) seeing

at 1.3 mm to this Gaussian fit. At a distance of ~ 73 pc, the disk resolved by the continuum would have a characteristic radial extent of about 36 AU (corresponding to the FWHM of the surface brightness distribution). Both the flux (360 ± 36 mJy) and spatial extent of the disk at 1.3 mm are consistent with ~ 40 K blackbody dust grains located at a distance of ~ 40 AU from the central binary (Kastner et al. 2008b²).

4. Modeling

4.1. CO line maps

To determine more precise values for the disk parameters, we employed standard modeling techniques previously used to interpret interferometric maps of molecular line emission (e.g., Qi et al. 2004; Raman et al. 2006; Hughes et al. 2008). Specifically, we used the Monte Carlo radiative transfer code RATRAN (Hogerheijde & van der Tak 2000) to solve for the CO level populations at each position within the disk and thereby to generate sky-projected emission-line images. These images were then passed to the MIRIAD task *uvmodel* to sample the model images at the same spatial frequencies as our SMA data. A minimum χ^2 is obtained by directly comparing the model and observed visibilities (Guilloteau & Dutrey 1998). The model geometry is that of a Keplerian disk in hydrostatic equilibrium with truncated power laws in density and temperature described (respectively) by $n(r) = n_{100}(\frac{r}{100\text{AU}})^{-p}$ and $T(r) = T_{100}(\frac{r}{100\text{AU}})^{-q}$, where $n(r)$ refers to the number (mid plane) density of H_2 and we assume $\text{CO}:\text{H}_2 = 10^{-4}$.

There are ten parameters that describe this Keplerian disk model (see Table 2). In practice, however, our modeling can constrain only five of these: the central mass, the systemic velocity (V_{LSR}), and the CO disk inclination (i), PA, and outer truncation radius (R_{out}). The modeling is relatively insensitive to the other parameters (T_{100} , q , n_{100} , p , and inner truncation radius R_{in}) because the $^{12}\text{CO}(2-1)$ emission imaged by the SMA is optically thick (Kastner et al. 2008b) and originates from the cooler, outer regions of the disk (the $^{13}\text{CO}(2-1)$ emission-line data are too noisy to provide useful constraints on the disk density structure parameters n_{100} and p). Furthermore, there is degeneracy between central mass and disk inclination; for the former, we initially adopted the total stellar mass of $1.8M_{\odot}$ determined by Stempels & Gahm (2004), then varied this parameter so as to explore the potential range of i in more detail (§4.2). The values of parameters T_{100} , q , n_{100} , p , and

²The value of ~ 80 AU quoted in Kastner et al. (2008b) is actually a diameter. The semi-major axis is ~ 40 AU.

R_{in} (Table 2) were fixed according to results obtained from models of the molecular disks orbiting other T Tauri stars (Dutrey et al. 1994, 1998). The remaining model parameters (V_{LSR} , P.A., i , R_{out}) were then varied in turn so as to ascertain best-fit values. The resulting set of best-fit model parameters and their formal 1- σ uncertainties are listed in Table 2. These uncertainties do not account for systematic errors (see below), as they were determined from the change in reduced χ^2 as the model parameters were varied; a representative contour plot of reduced χ^2 (illustrating its dependence on P.A. and i) is presented in Figure 5. The best-fit Keplerian disk model is presented in the form of synthetic velocity-resolved images in Fig 6 and as a position-velocity (P-V) diagram alongside the observed P-V diagram in Fig 7.

The value of $R_{out} = 370 \pm 30$ AU obtained from the model fitting confirms our earlier “eyeball” estimate. The systemic velocity we find from fitting the SMA data, 2.92 ± 0.01 km s $^{-1}$, is consistent with that determined from single-dish, mm-wave CO spectroscopy by Kastner et al. (2008b). The inferred disk inclination of $33.4 \pm 0.3^\circ$ is very similar to the value previously assumed in determining the masses of the components of the central binary system (see below). The position angle obtained from the best-fit model ($76.4 \pm 0.5^\circ$) is consistent with that derived from the elliptical gaussian fit to the continuum visibility ($73 \pm 5^\circ$). The truncated power law model generated by these best-fit parameters reproduces well the overall emission morphologies apparent in the velocity channel maps. There is some structure in the fit residuals (Fig 6), however. In particular, the data show an excess of emission from the southern portion of the disk relative to the model. The integrated line flux of the residuals is $\sim 14\%$ of the ^{12}CO and model fluxes (see Fig. 2). Given these systematics, and those due to the simplifying assumptions inherent in the molecular disk model, the formal errors listed in Table 2 likely somewhat underestimate the uncertainties in the best-fit model parameters.

4.2. Central binary system mass vs. disk inclination

Estimates of the total mass of the V4046 Sgr close binary, based on radial velocity curves obtained from optical spectroscopy of the double-lined system, range from $1.55 M_\odot$ (component masses $0.86 M_\odot$ and $0.69 M_\odot$; Quast et al. 2000) to $1.78 M_\odot$ (component masses $0.91 M_\odot$ and $0.87 M_\odot$; Stempels & Gahm 2004). Both estimates are based on an assumed binary system inclination of 35° (Quast et al. 2000). The Stempels & Gahm (2004) component masses appear to be more accurate, given the nearly equal radial velocity amplitudes of the two components and the improved agreement with pre-main sequence evolutionary tracks (see discussion in Stempels & Gahm 2004).

To ascertain the constraints placed by the SMA CO maps on both the mass of the central binary and the inclination of the disk, we fixed the remaining disk model parameters to their best-fit (Table 2) values, and allowed only central mass and inclination to vary. The results for reduced χ^2 , displayed in Fig. 8, illustrate the inherent degeneracy between mass and inclination; lower central masses and higher inclinations yield fits that are comparable in quality to those for higher central masses and lower inclinations. Nonetheless, this fitting exercise demonstrates that, for a central mass in the range 1.55 to 1.8 M_{\odot} allowed by the optical spectroscopy, the disk inclination is constrained to values between 33° and 37° . Given the similarity of these values of disk inclination to that assumed for the central binary in determining component masses from stellar radial velocities, it appears that the molecular disk is nearly coplanar with the central binary system. Although smaller central binary masses (and hence larger disk inclinations) are not precluded by our disk model fitting — indeed, we find that χ^2 reaches a minimum near $i \sim 40^{\circ}$, for a central mass of $\sim 1.4 M_{\odot}$ — values of central mass $\leq 1.5 M_{\odot}$ for this system lead to discord with pre-main sequence evolutionary tracks (Stempels & Gahm 2004).

4.3. Disk gas and dust masses

To estimate the disk molecular mass from the integrated SMA ^{12}CO and ^{13}CO line intensities (30.2 Jy km s $^{-1}$ for ^{12}CO and 8.7 Jy km s $^{-1}$ for ^{13}CO) we adopt the methods and assumptions described in Kastner et al. (2008a,b) and references therein. In particular, we assume optically thin ^{13}CO emission and CO:H $_2$ and $^{12}\text{C}:^{13}\text{C}$ ratios of 10^{-4} and 89, respectively; the latter values are highly uncertain. We assume the mean gas temperature is similar to that of the dust (37 K; see below). The ratio of the ^{12}CO and ^{13}CO line intensities indicates a ^{12}CO optical depth of ~ 26 . We use this result to infer a disk molecular mass of ~ 110 Earth masses from the ^{12}CO line intensity (see Equation 4 in Zuckerman et al. 2008). This gas mass estimate is consistent with that obtained for V4046 Sgr on the basis of single-dish (IRAM 30-m) data (Kastner et al. 2008b³). We note that the assumption that the ^{13}CO emission is optically thin is supported by the nondetection of C $^{18}\text{O}(2-1)$ emission by the SMA, although the large ^{12}CO optical depth places a lower limit on the ^{13}CO optical depth of ~ 0.4 .

Adopting a dust temperature of 37 K — obtained from a blackbody fit to the far-infrared/submillimeter spectral energy distribution of V4046 Sgr (Kastner et al. 2008b) —

³Due to a numerical transcription error, the gas mass estimate of ~ 13 Earth masses stated in Kastner et al. (2008b) is an order of magnitude too small.

and a dust opacity of $1.15 \text{ cm}^2 \text{ g}^{-1}$ (extrapolated from an opacity of $1.7 \text{ cm}^2 \text{ g}^{-1}$ at $880 \mu\text{m}$ assuming a dust opacity slope $\beta=1$; see Zuckerman et al. 2008), we estimate a disk dust mass of ~ 40 Earth masses. This is a factor of ~ 2 larger than the estimate obtained by Kastner et al. (2008b); the discrepancy is likely due to the adopted power-law dependence of opacity on wavelength.

5. Summary and Conclusions

Our $^{12}\text{CO}(2-1)$ and $^{13}\text{CO}(2-1)$ emission maps of V4046 Sgr reveal a rotating disk around this binary system extending out to a radius of ~ 370 AU. A truncated power-law fit to the $^{12}\text{CO}(2-1)$ visibilities indicate the disk is viewed at an inclination of 33° if the total central binary mass is $1.8 M_\odot$ (as determined by Stempels & Gahm 2004). However, we cannot rule out the possibility that the central binary mass is as small as $1.55 M_\odot$ (the value determined by Quast et al. 2000) on the basis of the SMA CO data alone, since disk inclinations as large as $\sim 40^\circ$ (corresponding to a central mass of $\sim 1.4 M_\odot$) are not precluded by the modeling.

While the position angle of the central binary is unknown, the close correspondence between the range of disk inclination determined from the modeling (§ 4.2) and the inclination of the binary star orbit adopted in previous binary system radial velocity studies (35° ; Quast et al. 2000) leads us to conclude that the binary pair and disk are nearly coplanar. The disk and orbital planes of circumbinary disk systems are expected to be very similar, because the system either formed with such an alignment or subsequently evolved into an aligned state (Monin et al. 2006). It is therefore significant that the disk and binary inclinations indeed appear to be aligned to within a few degrees, in this ~ 12 Myr-old system.

We resolved the 1.3 mm continuum emission from V4046 Sgr with the SMA, and find that the flux is consistent with 37 K dust located ~ 40 AU from the central stars (Kastner et al. 2008b). We estimate a mass of ~ 40 Earth masses of dust in the disk, about a factor of 3 smaller than the gas mass inferred from the CO line intensities (~ 110 Earth masses, assuming a CO:H₂ ratio of 10^{-4}). Hence, either the residual gas mass in the disk orbiting this rather “old” binary classical T Tauri system is much smaller than that expected for a gas-to-dust ratio of 100, or the disk is severely depleted in gas-phase CO. Indeed, for the temperature profile adopted here, $T < 20$ K for radii $\gtrsim 200$ AU, suggesting that much of the CO present in the disk may be in the form of icy grain mantles.

Although it appears most protoplanetary disks have dissipated after several million years (Haisch et al. 2001; Uzpen et al. 2009), V4046 Sgr, at age ~ 12 Myr, still retains a

substantial amount of mass in its circumbinary disk. Indeed, V4046 Sgr is one of only four known pre-main sequence stars within 100 pc that possess molecular disks. While V4046 Sgr is a close binary system, the other three (TW Hya, HD 141569, and 49 Ceti) do not appear to harbor close companions. Previous submillimeter studies have revealed gas-rich disks extending out to about 200 AU in both TW Hya and 49 Ceti (Qi et al. 2004; Hughes et al. 2008) and ~ 250 AU in HD 141569 (Dent et al. 2005). Our SMA imaging demonstrates that the V4046 Sgr disk (radius 370 AU) is even larger and, when compared to the disk orbiting TW Hya (a single star of slightly later spectral type), also retains a larger gas mass (if we apply the same standard assumptions of CO abundance relative to H_2 of 10^{-4} and $^{12}\text{C}/^{13}\text{C}$ of 89). The twin stars in V4046 Sgr evidently are still actively accreting from this extensive, gaseous disk and, likewise, any young Jovian planets within this system may be undergoing their final stages of gas accretion.

Giant planet formation in disks can occur in one of two ways: core accretion, with timescales of a few $\times 10^6$ years (Inaba et al. 2003; Lissauer et al. 2009) or disk instability, with timescales as short as a few $\times 10^3$ years (Boss 2000). One expects that long-lived disks such as those around TW Hya and V4046 Sgr (ages ~ 10 Myr) will provide more opportunities to form giant planets than shorter-lived disks, regardless of how they form, so long as sufficient reservoirs of gas remain present. Meanwhile, studies have shown that disks around close (< 100 AU) binary systems tend to dissipate faster than those around single stars or more widely separated systems (Bouwman et al. 2006; Cieza et al. 2009). Typically, therefore, if giant planets are to form around close binary systems, they must form more rapidly than would be necessary for giant planets forming around single stars. Indeed, there is evidence that planets in binary systems with separations < 100 AU are biased towards higher masses, possibly as a natural consequence of rapid planet formation via gravitational instability (Duchêne 2010).

V4046 Sgr therefore presents a particularly interesting and important case. Given its tight ($\sim 9 R_\odot$) separation, the outer portions of its circumbinary disk, where giant planets are expected to form, will have been left relatively undisturbed throughout the system’s lifetime. Only within ~ 1 AU are dynamical effects due to the central binary expected to significantly affect the disk (Jensen & Mathieu 1997 estimate that an inner hole out of radius ~ 0.2 AU is necessary to account for the lack of excess infrared emission from V4046 Sgr shortward of $10 \mu\text{m}$). While about 20% of extrasolar planets have been detected in binary systems (Raghavan et al. 2006; Eggenberger et al. 2007), no unambiguous detection of an extrasolar planet has been made for a binary with separation < 20 AU (though the eclipse timings of HW Virginis and CM Draconis suggest that planets may orbit these two binaries; Deeg et al. 2008; Lee et al. 2009). Hence, there is ample motivation to continue to scrutinize the V4046 Sgr disk at the highest possible spatial resolution, to see if planets are already orbiting this

binary system.

Acknowledgements. We thank Ben Zuckerman for useful discussions and comments and Meredith Hughes for lending us her deprojected visibility code. We are grateful to Michiel Hogerheijde for providing access to the 2D version of RATRAN used in this work. We appreciate the suggestions and comments of the anonymous referee. The Submillimeter Array is a joint project between the Smithsonian Astrophysical Observatory and the Academia Sinica Institute of Astronomy and Astrophysics and is funded by the Smithsonian Institution and the Academia Sinica. This research was supported by NASA Astrophysics Data Analysis Program grant NNX09AC96G to RIT and UCLA.

REFERENCES

- Bary, J. et al. 2008, ApJ, 678, 1088
- Beckwith, S., & Sargent, A. 1993, ApJ, 402, 280
- Bitner, M., et al. 2007, ApJ, 661, L69
- Bitner, M., et al. 2008, ApJ, 688, 1326
- Boss, A. P. 2000, ApJ, 536, L101
- Bouwman, J., Lawson, W. A., Dominik, C., Feigelson, E. D., Henning, T., Tielens, A. G. G. M., & Waters, L. B. F. M. 2006, ApJ, 653, L57
- Brittain, S. D., Najita, J. R., & Carr, J. S. 2009, ApJ, 702, 85
- Cieza, L. A., et al. 2009, ApJ, 696, L84
- Ehrenfreund, P. & Charnley, S.B. 2000, ARA&A, 38, 427
- Deeg, H. J., Ocaña, B., Kozhevnikov, V. P., Charbonneau, D., O'Donovan, F. T., & Doyle, L. R. 2008, A&A, 480, 563
- Dent, W. R. F., Greaves, J. S., & Coulson, I. M. 2005, MNRAS, 359, 663
- Duchêne, G. 2010, ApJ, 709, L114
- Dullemond, C. P., Hollenbach, D., Kamp, I., & D'Alessio, P. 2007, Protostars and Planets V, 555

- Dutrey, A., Guilloteau, S., & Simon, M. 1994, *A&A*, 286, 149
- Dutrey, A., Guilloteau, S., Prato, L., Simon, M., Duvert, G., Schuster, K., & Ménard, F. 1998, *A&A*, 338, L63
- Eggenberger, A., Udry, S., Chauvin, G., Beuzit, J.-L., Lagrange, A.-M., Ségransan, D., & Mayor, M. 2007, *A&A*, 474, 273
- Glassgold, A.E., Meijerink, R., Najita, J.R. 2009, *ApJ*, 701, 142
- Guilloteau, S., & Dutrey, A. 1998, *A&A*, 339, 467
- Haisch, K. E., Jr., Lada, E. A., & Lada, C. J. 2001, *ApJ*, 553, L153
- Ho, P. T. P., Moran, J. M., & Lo, K. Y. 2004, *ApJ*, 616, L1
- Hogerheijde, M. R., & van der Tak, F. F. S. 2000, *A&A*, 362, 697
- Hughes, A.M., Wilner, D.J., Kamp, I., & Hogerheijde, M.R. 2008, *ApJ*, 681, 626
- Hubbard, W.B., Burrows, A., & Lunine, J.I. 2002, *ARA&A*, 40, 103
- Inaba, S., Wetherill, G. W., & Ikoma, M. 2003, *Icarus*, 166, 46
- Jensen, E. L. N., & Mathieu, R. D. 1997, *AJ*, 114, 301
- Kastner, J. H., Zuckerman, B., Weintraub, D. A., & Forveille, T. 1997, *Science*, 277, 67
- Kastner, J.H., Zuckerman, B., & Forveille, T. 2008a, *A&A*, 486, 239
- Kastner, J.H., Zuckerman, B., Hily-Blant, P., & Forveille, T. 2008b, *A&A*, 492, 469
- Lee, J. W., Kim, S.-L., Kim, C.-H., Koch, R. H., Lee, C.-U., Kim, H.-I., & Park, J.-H. 2009, *AJ*, 137, 3181
- Lissauer, J. J., Hubickyj, O., D'Angelo, G., & Bodenheimer, P. 2009, *Icarus*, 199, 338
- Luu, J.X., & Jewitt, D.C. 2002, *ARA&A*, 40, 63
- Monin, J.-L., Clarke, C.J., Prato, L., & McCabe, C. 2006, *Protostars and Planets V*, 395
- Najita, J.R., Crockett, N., & Carr, J.S. 2008, *ApJ*, 687, 1168
- Najita, J.R., et al. 2010, *ApJ*, 712, 274
- Papaloizou, J.C.B. & Nelson, R.P. 2005, *A&A*, 433, 247

- Qi, C., Ho, P.T.P., Wilner, D.J., et al. 2004, ApJ, 616, L11
- Qi, C., Wilner, D.J., Calvet, N., et al. 2006, ApJ, 636, L157
- Qi, C., Wilner, D.J., Aikawa, Y., et al. 2008, ApJ, 681, 1396
- Quast, G.R., Torres, C.A.O., de la Reza, R., et al. 2000, in Proc. of IAU Symp. 200, p. 28
- Raghavan, D., Henry, T. J., Mason, B. D., Subasavage, J. P., Jao, W.-C., Beaulieu, T. D., & Hambly, N. C. 2006, ApJ, 646, 523
- Raman, A., Lisanti, M., Wilner, D. J., Qi, C., & Hogerheijde, M. 2006, AJ, 131, 2290
- Salyk, C. et al. 2007, ApJ, 655, L105
- Stempels, H. C. & Gahm, G. F. 2004, A&A, 421, 1159
- Thi, W.-F., van Zadelhoff, G.-J., & van Dishoeck, E.F. 2004, A&A, 425, 955
- Thommes, E. W., Matsumura, S., & Rasio, F. A. 2008, Science, 321, 81
- Torres, C.A.O., Quast, G.R., Melo, C.H.F., & Sterzik, M.F. 2008, in *Handbook of Star Forming Regions*, ed. B. Reipurth, Astron. Soc. Pacific, San Francisco
- Uzpen, B., Kobulnicky, H. A., & Kinemuchi, K. 2009, AJ, 137, 3329
- Weinberger, A. J., Rich, R. M., Becklin, E. E., Zuckerman, B., & Matthews, K. 2000, ApJ, 544, 937
- Zuckerman, B., Forveille, T., & Kastner, J.H. 1995, Nature, 373, 494
- Zuckerman, B. 2001, ARA&A, 39, 549
- Zuckerman, B., Melis, C., Song, I., et al. 2008, ApJ, 683, 1085

Table 1: Observational Parameters

Parameter	$^{12}\text{CO}(2-1)$	$^{13}\text{CO}(2-1)$	$\text{C}^{18}\text{O}(2-1)$	Continuum 1.3mm
Rest Frequency (GHz)	230.538	220.399	219.560	225
Beam Size (FWHM)	$2.24'' \times 1.48''$	$2.34'' \times 1.66''$	$2.35'' \times 1.67''$	$1.67'' \times 1.01''$
P.A.	8°	4°	4°	1°
RMS noise (mJy beam $^{-1}$)	87	76	76	0.8
Peak Flux Density (mJy beam $^{-1}$)	2640	790	<300	210.5
Integrated Line Intensity (Jy km s $^{-1}$)	30.2	8.7	<1	–
Integrated Continuum Flux (mJy)	–	–	–	360

Table 2: Model Properties

Parameter	Value
Central mass (M_\odot)	1.8^a
Inclination ($^\circ$)	33.4 ± 0.3
Systemic LSR Velocity (km s $^{-1}$)	2.92 ± 0.01
P.A. ($^\circ$)	76.4 ± 0.5
R_{in} (AU)	4^b
R_{out} (AU)	370 ± 30
n_{100} (cm $^{-3}$)	4×10^8 b
p	2^b
T_{100} (K)	28^b
q	0.6^b

^aSee § 4.2

^bAdopted values; these are not fit.

Quoted uncertainties are 1σ . See text for more details.

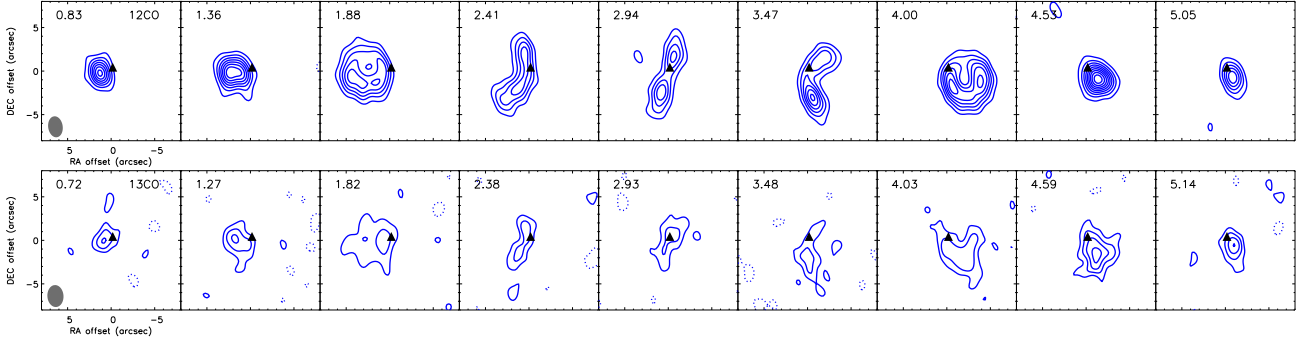


Fig. 1.— SMA velocity-resolved maps of V4046 Sgr in $^{12}\text{CO}(2-1)$ (top) and $^{13}\text{CO}(2-1)$ (bottom). The contour levels are $0.09 \text{ mJy/beam} \times [3, 6, 9, \dots]$ for $^{12}\text{CO}(2-1)$ and $0.08 \text{ mJy/beam} \times [-2, 2, 4, 6, \dots]$ for $^{13}\text{CO}(2-1)$ with dotted lines representing the negative contours. In each frame, the central velocity (in km s^{-1} with respect to the Local Standard of Rest (LSR)) is indicated at upper left; the position of the continuum source centroid is indicated by a small black triangle; and the synthesized beam size, shape, and position angle is indicated by the grey shaded ellipse at lower left.

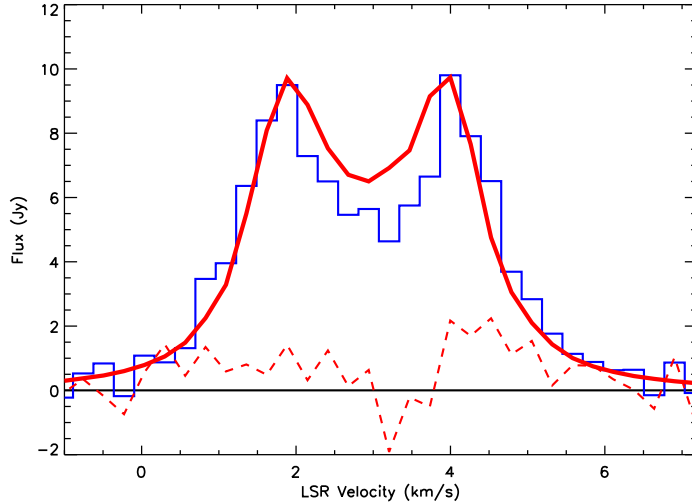


Fig. 2.— Line profile of $^{12}\text{CO}(2-1)$ obtained from the SMA images of the V4046 Sgr disk. Overlaid in bold is the best-fit model as described in § 4. The dotted line shows the residual when the model is subtracted from the data in the visibilities.

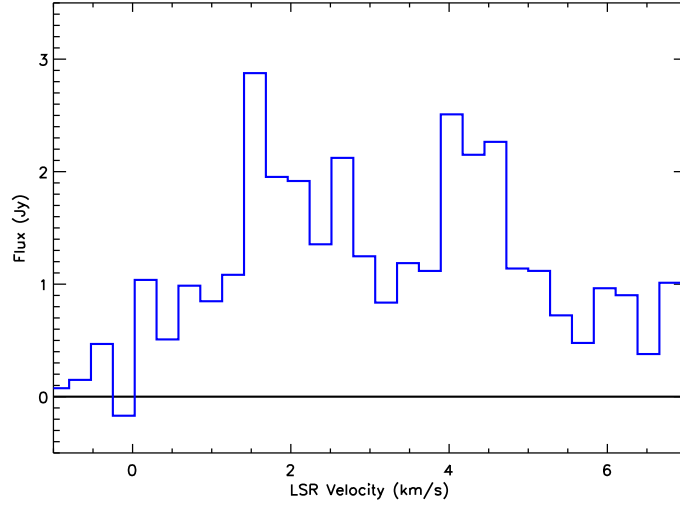


Fig. 3.— Line profile of $^{13}\text{CO}(2-1)$ obtained from the SMA images of the V4046 Sgr disk.

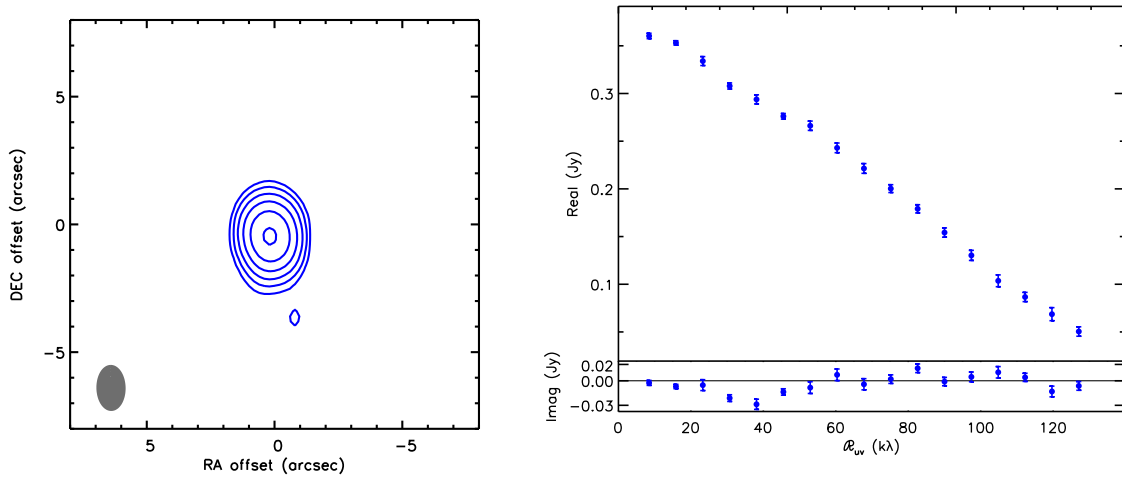


Fig. 4.— Continuum emission map (left) and deprojected visibility plot (right). The decline in the real component of the visibility as a function of baseline is a characteristic of resolved structures. The FWHM corresponds to a radial extent of about 36 AU, consistent with the characteristic extent of 40 K dust grains in the system.

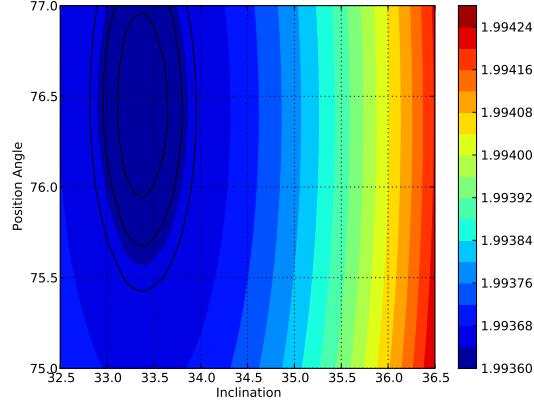


Fig. 5.— Contour maps of reduced χ^2 for a systemic velocity of 2.92 km s^{-1} and outer radius of 370 AU. The black ellipses indicate 1-, 3-, and 5- σ contours.

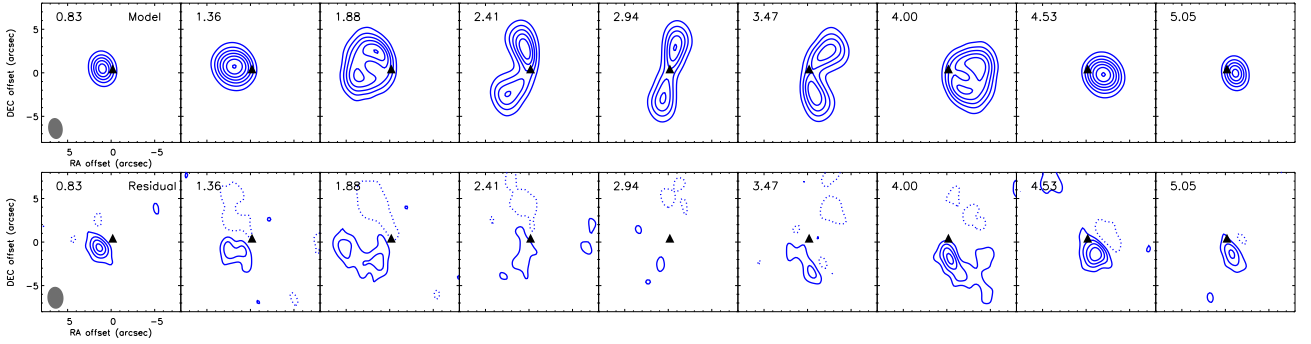


Fig. 6.— $^{12}\text{CO}(2-1)$ best-fit model map (top) and residual map (bottom). In each frame, the central velocity (km s^{-1}) is indicated at upper left; the position of the continuum source centroid is indicated by a small black triangle; and the synthesized beam size ($2.3'' \times 1.6''$ at 8.5°) is indicated by the grey shaded ellipse at lower left. Contours levels are $0.09 \text{ mJy/beam} \times [-3, 3, 6, 9, \dots]$ for both panels with dotted contours for the negative levels. Figure 2 illustrates how the residual flux varies over velocity. The integrated line flux of the residuals is $\sim 14\%$ of the ^{12}CO and model fluxes.

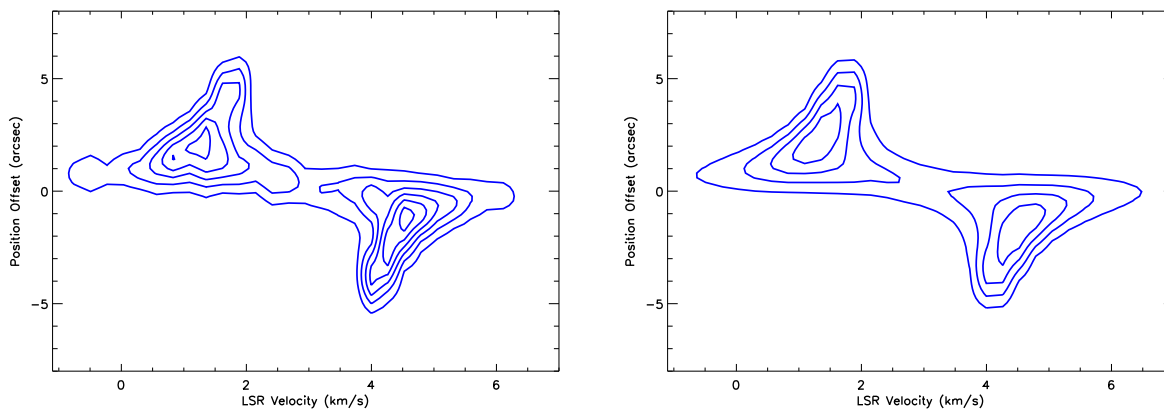


Fig. 7.— Position-velocity diagram for the $^{12}\text{CO}(2-1)$ emission in V4046 Sgr (left) and the best-fit Keplerian model (right). Both diagrams were constructed for a P.A. cut of 76.4° through the position of the central binary star.

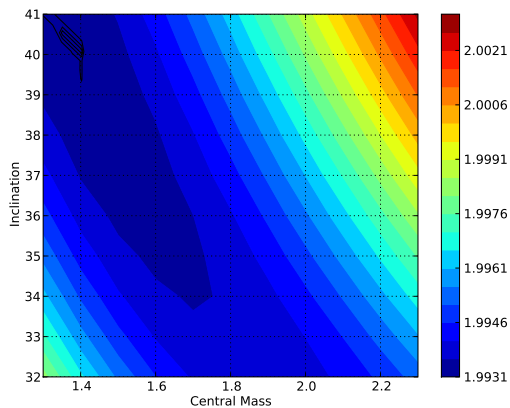


Fig. 8.— Contour plot of reduced χ^2 for disk inclination vs. central (stellar) mass. The black contours indicate 1-, 3-, and 5- σ contours; the jagged appearance is due to the coarseness of the grid used. The range of central masses covered in the plot is significantly larger than that determined via studies of stellar radial velocities ($1.55\text{--}1.8 M_\odot$; Quast et al. 2000; Stempels & Gahm 2004) under the assumption of a binary inclination of 35° .